IJICTR
International Journal of Information & Communication Technology Research

Volume 11- Number 2 – Spring 2019 (18 -28)

Wireless-Powered Cooperative Spectrum Sharing Networks with Full-Duplex and NOMA Transmissions

Azar Hakimi
Faculty of Engineering
SKU University
Shahrekord, Iran
Hakimi@stu.sku.ac.ir

Mohammadali Mohammadi*, Zahra Mobini
Faculty of Engineering
SKU University
Shahrekord, Iran
{m.a.mohammadi, z.mobini}@sku.ac.ir

Received: 10 August 2018 - Accepted: 22 April 2019

Abstract— **We consider a non-orthogonal multiple access (NOMA) cooperative spectrum sharing network, where a multi-antenna secondary transmitter assists transmission of a primary transmitter-receiver pair, and at the same time transmits to a secondary receiver. The secondary transmitter is assumed to be full-duplex and energy-constrained. Therefore, secondary transmitter replenishes its battery storage via energy harvesting from an energy access point located in its vicinity. In order to cancel the self-interference at the secondary transmitter, two zero-forcing (ZF)-based beamforming schemes and one maximum ratio combining/maximum ratio transmission (MRC/MRT) scheme are designed. Then, corresponding outage probability analysis of the primary and secondary networks with proposed beamforming schemes are derived. Outage probability results are used to study the delay-constrained throughput of the system. Our results suggest that by utilizing ZF-based beamforming schemes, significant performance improvement can be achieved compared to the half-duplex counterpart. Moreover, our results indicate that proposed ZF-based schemes achieves a zero-diversity order.**

Keywords-component; Non-orthogonal multiple access (NOMA); cooperative spectrum sharing networks; full-duplex, delay-constrained throughput; zero-forcing beamforming.

I. INTRODUCTION

Full-duplex (FD) communication, which is potentially able to double the spectral efficiency as compared with the half-duplex (HD) counterpart, has been recently touted as a promising technology in the emerging wireless communication systems such as fifth generation (5G) cellular networks due to its potential [1]. However, the key challenge in practical FD systems is the residual self-interference (SI) which considerably limits its application [2]. To overcome the SI, several analog and digital domain SI cancellation techniques have been proposed in the literature [1]. Analog domain SI suppression is performed using passive isolation techniques such as placing radio frequency (RF) absorber material between antennas and use of narrow beam width directional antennas [2]. Digital SI cancellation is applied after analog SI cancellation reduce the SI signals as low as the receiver noise floor. Recent advances in SI cancellation methods have made FD transceivers feasible in practice. Specifically, single antenna FD

* Corresponding Author

implementations rely on analog SI cancellation, digital SI cancellation, and antenna based SI suppression [3]. In case of multi-antenna systems, spatial suppression through applying zero-forcing (ZF), null-space projection and antenna selection has received a lot of research interest to efficiently suppress/cancel SI [4]-[6].

Cognitive radio (CR) is another promising candidate to improve the spectral efficiency of the future mobile communication system. In the CR networks, secondary users (SUs) can access the primary users' (PUs) licensed spectrum via underlay or overlay strategies [7]. In the underlay strategy, the SUs are allowed to transmit over PUs spectrum as long as they meet the interference constraint of the PUs. In overlay networks, SUs cooperatively assists the PUs and in return they are allowed to simultaneously transmit over the licensed spectrum [8]. Furthermore, by adopting FD nodes, remarkable improvement in spectral efficiency over CR networks can be achieved [9]. A survey of research on FD enabled CR networks has been provided in [10].

On the other hand, non-orthogonal multiple access (NOMA) has gained more attention as a candidate multiple access technique in 5G for simultaneously serving multiple users over the same spectrum [11]-[14]. Users that are exposed to lack of spectrum or have week channel conditions can cooperate with NOMA users and transmit over the same spectrum. NOMA techniques are primarily classified into two categories, namely, code-domain NOMA and power-domain NOMA [12]. Power-domain NOMA multiplexes multiple users at the transmitter with different power levels and deploys multiuser detection algorithms such as successive interference cancellation (SIC) at the receivers to decode the received signals. The integration of NOMA with CR networks has been investigated in a few recent studies [15]-[18]. Specifically, the authors in [15] investigated multicast/unicast transmissions in a downlink CR-NOMA system. The authors in [16] studied the application of NOMA in large-scale CR networks by using tools from stochastic geometry. A cooperative mechanism for a NOMA-assisted multicast CR network has been proposed in [17]. In [18], a cooperative NOMA system was analyzed wherein an access point (AP) communicates to one SU via the help of a dedicated FD multi-antenna relay, while at the same time the AP directly transmits to a SU.

Meanwhile, energy efficiency is also an important concern in 5G [19]. In this regard, radio frequency (RF) energy harvesting is a promising approach to improve the energy efficiency, where directed RF signals are used to power the wireless devices [20]. In this context, two main approaches have been investigated in the literature known as (ii) simultaneous wireless information and power transfer (SWIPT) and (i) wireless power transfer (WPT). WPT refers to case where dedicated external energy sources such as energy access point (EAP) are deployed to power wireless devices, while in SWIPT, source's signal conveys both energy and information to the energy-constraint receiver. Performance of an energy-constrained cooperative NOMA system has been studied in [21], at which NOMA near user is wirelessly powered to relay the far user's information. A wirelessly-powered NOMA system has been studied in [22], where an FD transmitter harvests energy from a dedicated energy source and its own loop channel, while transmits information to the NOMA users at the same time.

Motivated by the energy efficiency and energy efficiency requirements of the 5G wireless networks we integrate the FD communications, NOMA technique, and WPT into cooperative spectrum sharing network. Specifically, an energy-constraint FD multi-antenna secondary transmitter (STx) is deployed as a relay to serve both primary-receiver (PRx) and secondary-receiver (SRx) at the same time by using NOMA transmission. STx powers its battery storage from RF signals transmitted by a dedicated EAP.

The main contributions of this paper are as follows:

- We propose two zero forcing (ZF)-based beamforming designs to mitigate the SI at the FD STx. Delay-constrained throughput expressions for the proposed beamforming designs are derived. Furthermore, we develop the system's delay-constrained throughput of a benchmark scenario, where maximum ratio combining (MRC) and maximum ratio transmission (MRT) principles are used the receive and transmit beamformer design.
- High signal-to-noise ratio (SNR) approximations of the outage probability are presented for the proposed beamforming designs, which facilitate gaining insights into the impact of the system parameters on the system performance.
- We further analyze the HD spectrum sharing counterpart in terms of the outage probability and delay-constraint throughput, to illustrate the gains achieved by the FD operation.

Notation: Bold upper case letters are used to denote matrices; bold lower case letters are used to denote vectors. The superscripts $(\cdot)^T$, $(\cdot)^\dagger$, $(\cdot)^*$, and $\|\cdot\|$ stand for transpose, conjugate transpose, conjugate, and the Euclidean norm of the vector, respectively; $\Pr(A)$ denotes the probability of event A; $\bar{A}$ denotes the complementary event of A; $F_X(\cdot)$ and $f_X(\cdot)$ denote the cumulative distribution function (cdf) and probability density function (pdf) of the random variable (RV) X, respectively; $\mathbb{E}\{x\}$ stands for the expectation of the random variable x; $\mathcal{CN}(0,\sigma^2)$ denotes a circularly symmetric complex Gaussian RV x with variance σ^2; $\Gamma(a)$ is the Gamma function; $\Gamma(a,x)$ and $\gamma(a,x)$ is upper incomplete and lower incomplete Gamma function, respectively [23, Eq.(8.350)]; $K_\nu(\cdot)$ is the νth order modified Bessel function of the second kind [23, Eq. (8.432)]; $W_{\lambda,\mu}(\cdot)$ is the Whittaker function [23, Eq. (9.222)]

II. SYSTEM MODEL

As illustrated in Fig. 1, we consider a spectrum sharing network in which a PTx and an STx communicate with their receivers PRx and SRx, respectively. However, due to the high path-loss and

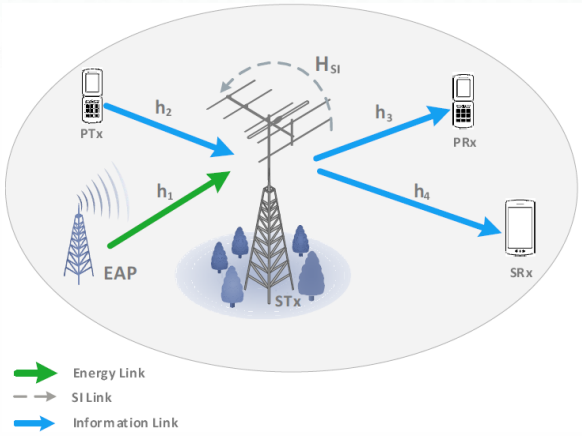

Fig 1. System model.

heavy shadowing, direct link between the PTx and the PRx is not available. It is assumed that the STx acts as an intermediate node and relays the primary message, and instead, it simultaneously reaches the spectrum by using NOMA. In other words, using NOMA allows the STx to serve both PRx and SRx at the same time and on the same channel. Each node is equipped with a single antenna, except the STx that is equipped with N_T antennas to transmit signals and N_R antennas to receive signals. Besides, we consider that the STx is an energy-constrained node and refills its battery via a dedicated EAP. For this purpose, the STx employs a time-switching (TS) protocol [6]. We further assume that the PRx is located in the vicinity of the STx at distance d_3, while the SRx is located far from the STx at distance d_4 ($d_4 > d_3$).

All network's channels are assumed to undergo flat Rayleigh fading. Therefore, all channels remain constant during each block of transmission but vary independently over different blocks. Let $\mathbf{h}_1 \in \mathcal{C}^{N_R \times 1}$, $\mathbf{h}_2 \in \mathcal{C}^{N_R \times 1}$, $\mathbf{h}_3 \in \mathcal{C}^{N_T \times 1}$, and $\mathbf{h}_4 \in \mathcal{C}^{N_R \times 1}$ denote the channel spanning from EAP to STx, from PRx to STx, from STx to PRx, and from STx to SRx, respectively. The entries of $\mathbf{h}_i$, $i \in \{1,2,3,4\}$ are assumed to be independent identically distributed (i.i.d) zero mean complex Gaussian RVs with variance β_{h_i}, which models the path loss effect for the corresponding link.

A. Energy Harvesting Phase

The first phase of transmission is devoted to harvesting energy at the STx using TS protocol. At α fraction of the transmission block time T, i.e., αT, the STx harvests energy from the EAP, where $0 \leq \alpha \leq 1$. Hence, during the first phase the received signal at the STx can be expressed as

$$y_{\mathrm{ST},1}[i] = \sqrt{\beta_{h_1} P_{\mathrm{EA}}}\mathbf{w}_E^{\dagger}\mathbf{h}_1 x_e[i] + \mathbf{w}_E^{\dagger}\boldsymbol{n}_{\mathrm{ST}}[i], \qquad (1)$$

where P_{EA} denotes the EAP's transmit power, $x_e[i]$ is the energy symbol transmitted from EAP, $\mathbf{w}_E \in \mathcal{C}^{N_R \times 1}$ is the energy beamformer at the STx, and $\boldsymbol{n}_{\mathrm{ST}}[i] \sim \mathcal{CN}(0, \sigma_{\mathrm{ST}}^2 \boldsymbol{I}_{N_R})$ denotes the additive white Gaussian noise (AWGN) at STx.

Similar to [6], we ignore the amount of harvested energy from the noise. Thus, the harvested energy and subsequently the transmit power at the STx are obtained as

$$E_{\mathrm{ST}} = \left(\eta \beta_{h_1} P_{\mathrm{EA}} |\mathbf{w}_E^{\dagger}\mathbf{h}_1|^2\right)\alpha T, \qquad (2)$$

and

$$P_{\mathrm{ST}} = \kappa \beta_{h_1} P_{\mathrm{EA}} |\mathbf{w}_E^{\dagger}\mathbf{h}_1|^2, \qquad (3)$$

respectively, where $\kappa = \frac{\eta\alpha}{1-\alpha}$ and η denotes the RF-to-DC conversion efficiency. It can readily show that the optimal $\mathbf{w}_E$ in order to maximize the harvested power at the STx, is $\mathbf{w}_E = \frac{\mathbf{h}_1}{\|\mathbf{h}_1\|}$, which results in $P_{\mathrm{ST}} = \kappa \beta_{h_1} P_{\mathrm{EA}} \|\mathbf{h}_1\|^2$.

B. Information Transfer Phase

In the information transfer phase, PTx sends its message to the STx in the remained time, $(1-\alpha)T$. Therefore, during the second phase, the received signal at the STx can be expressed as

$$y_{\mathrm{ST},2}[i] = \sqrt{\beta_{h_2} P_{\mathrm{PT}}}\mathbf{w}_r^{\dagger}\mathbf{h}_2 x_{\mathrm{PR}}[i] + \mathbf{w}_r^{\dagger}\mathbf{H}_{\mathrm{SI}}\mathbf{w}_t x_R[i] + \mathbf{w}_r^{\dagger}\boldsymbol{n}_{\mathrm{ST}}[i], \qquad (4)$$

where P_{PT} is the transmit power of PTx, $\mathbf{w}_r \in \mathcal{C}^{N_R \times 1}$ and $\mathbf{w}_t \in \mathcal{C}^{N_T \times 1}$ are the receiver and transmit beamformers at the FD STx, respectively, and $x_{\mathrm{PR}}[i]$ is the transmit signal of the PTx. $x_R[i] = \sqrt{a_1 P_{\mathrm{ST}}} x_{\mathrm{PR}}[i] + \sqrt{a_2 P_{\mathrm{ST}}} x_{\mathrm{SR}}[i]$ denotes the superimposed signal that the STx, transmits to the receivers where $x_{\mathrm{SR}}[i]$ is the information symbol intended for SRx, P_{ST} is the transmit power of STx, and a_i are the power allocation coefficients, such that $a_1 + a_2 = 1$ and $a_1 < a_2$ (since we assume that SRx is located farther to STx than PRx and needs more power allocation coefficient to decodes its message). Similar to [4], we model the elements of the $N_R \times N_T$ SI channel $\mathbf{H}_{\mathrm{SI}}$ as i.i.d. $\mathcal{CN}(o, \sigma_{\mathrm{SI}}^2)$ RVs.

Accordingly, the received signal-to-interference-plus-noise ratio (SINR) at the STx can be written as

$$\gamma_{\mathrm{ST}} = \frac{\beta_{h_2} P_{\mathrm{PT}} |\mathbf{w}_r^{\dagger}\mathbf{h}_2|^2}{\kappa \beta_{h_1} P_{\mathrm{EA}} \|\mathbf{h}_1\|^2 |\mathbf{w}_r^{\dagger}\mathbf{H}_{\mathrm{SI}}\mathbf{w}_t|^2 + \sigma_{\mathrm{ST}}^2}. \qquad (5)$$

Eq. (5) represents the required SINR at the STx to decode PTx's information. Then, the STx superimposes its message with PTx's information decoded at the STx and transmits it to the PRx and SRx. In Eq. (5) we used the fact that $\mathbb{E}\{x_{\mathrm{PR}} x_{\mathrm{PR}}^*\} = \mathbb{E}\{x_{\mathrm{SR}} x_{\mathrm{SR}}^*\} = 1$. As a result, in the second phase, PRx and SRx receive signals as following

$$y_{\mathrm{PR}}[i] = \sqrt{\beta_{h_3} P_{\mathrm{ST}}}\mathbf{h}_3^T \mathbf{w}_t x_R[i] + n_{\mathrm{PR}}[i], \qquad (6)$$

and

$$y_{\mathrm{SR}}[i] = \sqrt{\beta_{h_4} P_{\mathrm{ST}}}\mathbf{h}_4^T \mathbf{w}_t x_R[i] + n_{\mathrm{SR}}[i], \qquad (7)$$

respectively, where $n_{\mathrm{PR}}[i] \sim \mathcal{CN}(0, \sigma_{\mathrm{PR}}^2)$ and $n_{\mathrm{SR}}[i] \sim \mathcal{CN}(0, \sigma_{\mathrm{SR}}^2)$ are AWGN at the PRx and the SRx, respectively. Based on NOMA principals, successive interference cancellation (SIC) is performed at the PRx, since it has better channel condition, in order to detect and subtract its counterpart message from its received signal. Then, PRx decodes

its own message from the remained signal. Thus, the received SINR at the PRx to detect SRx's message, x_{SR}, is given by

$$\gamma_{\mathrm{PR},x_{\mathrm{SR}}} = \frac{\beta_{h_3}\beta_{h_1}a_2\kappa P_{\mathrm{EA}}\|\mathbf{h}_1\|^2|\mathbf{h}_3^T\mathbf{w}_t|^2}{\beta_{h_3}\beta_{h_1}a_1\kappa P_{\mathrm{EA}}\|\mathbf{h}_1\|^2|\mathbf{h}_3^T\mathbf{w}_t|^2+\sigma_{\mathrm{PR}}^2}. \quad (8)$$

Consequently, the desired information of PTx can be achieved after decoding and subtracting the x_{SR} from the received signal at the PTx. Thus, the desired SNR at PRx for decoding its own signal is given by

$$\gamma_{\mathrm{PR}} = \frac{\beta_{h_3}\beta_{h_1}a_1\kappa P_{\mathrm{EA}}}{\sigma_{\mathrm{PR}}^2}\|\mathbf{h}_1\|^2|\mathbf{h}_3^T\mathbf{w}_t|^2. \quad (9)$$

Based on the NOMA nature, the user that suffers poor channel condition considers its counterpart message as interference and decodes its message. Subsequently, the required SINR at the SRx to decode its massage is as following

$$\gamma_{\mathrm{SR}} = \frac{\beta_{h_4}\beta_{h_1}a_2\kappa P_{\mathrm{EA}}\|\mathbf{h}_1\|^2|\mathbf{h}_4^T\mathbf{w}_t|^2}{\beta_{h_4}\beta_{h_1}a_1\kappa P_{\mathrm{EA}}\|\mathbf{h}_1\|^2|\mathbf{h}_4^T\mathbf{w}_t|^2+\sigma_{\mathrm{SR}}^2}. \quad (10)$$

III. BEAMFORMING DESIGN

In this section, we provide low complexity joint receive/transmit beamforming designs for end-to-end SINR maximization. Specifically, based on ZF SI cancellation, receive/transmit beamforming vectors at the STx are designed [5], [6].

A. TZF Scheme

We apply MRC at the STx input, i.e., $\mathbf{w}_r^{\mathrm{MRC}} = \frac{\mathbf{h}_2}{\|\mathbf{h}_2\|}$ and then by substituting $\mathbf{w}_r^{\mathrm{MRC}}$ into (5), the transmit beamforming vector at the STx can be obtained using the ZF criterion such that

$$\max_{\|\mathbf{w}_t\|=1} |\mathbf{h}_3^T\mathbf{w}_t|^2, \quad \text{s.t} \quad \mathbf{h}_2^\dagger\mathbf{H}_{\mathrm{SI}}\mathbf{w}_t = 0. \quad (11)$$

Following similar steps in [6], it can be readily checked that $\mathbf{B} \triangleq \mathbf{H}_{\mathrm{SI}}^\dagger\mathbf{h}_2\mathbf{h}_2^\dagger\mathbf{H}_{\mathrm{SI}}$ is a rank-one Hermitian matrix with eigenvalue $\lambda \triangleq \|\mathbf{h}_2^\dagger\mathbf{H}_{\mathrm{SI}}\|^2$ and eigenvector $\boldsymbol{x} \triangleq \frac{\mathbf{H}_{\mathrm{SI}}^\dagger\mathbf{h}_2}{\|\mathbf{H}_{\mathrm{SI}}^\dagger\mathbf{h}_2\|}$. Accordingly, by using the eigenvalue decomposition of $\mathbf{B}$, i.e., $\boldsymbol{x}^\dagger\left(\boldsymbol{I}-\frac{1}{\lambda}\mathbf{B}\right)=0$ we get $\boldsymbol{x}^\dagger\left(\boldsymbol{I}-\frac{1}{\lambda}\mathbf{B}\right)\bar{\mathbf{w}}_t = 0$ for all $\bar{\mathbf{w}}_t \neq \mathbf{0}$. Comparing this with the ZF constraint in (11), we obtain $\mathbf{w}_t = \mathbf{C}\bar{\mathbf{w}}_t$, where $\mathbf{C} = \boldsymbol{I}_{N_T} - \frac{\mathbf{H}_{\mathrm{SI}}^\dagger\mathbf{h}_2\mathbf{h}_2^\dagger\mathbf{H}_{\mathrm{SI}}}{\|\mathbf{h}_2^\dagger\mathbf{H}_{\mathrm{SI}}\|^2}$, without violating the ZF constraint. Therefore, the objective function in (11) reduces to $|\mathbf{h}_3^T\mathbf{C}\bar{\mathbf{w}}_t|^2$ which is maximized with $\bar{\mathbf{w}}_t = k_c\mathbf{C}\mathbf{h}_3^*$. Note that $\mathbf{C}$ is an idempotent matrix and hence $\mathbf{C} = \mathbf{C}^2$. Moreover, since $||\mathbf{w}_t|| = 1$, it is clear that $k_c = \frac{1}{\|\mathbf{C}\mathbf{h}_3^*\|}$. Consequently, the transmit beamformer for the TZF scheme is

$$\mathbf{w}_t^{\mathrm{ZF}} = \frac{\mathbf{C}\mathbf{h}_3^*}{\|\mathbf{C}\mathbf{h}_3^*\|}. \quad (12)$$

B. RZF Scheme

With RZF scheme, we set $\mathbf{w}_t$ according to MRT concept, i.e., $\mathbf{w}_t^{\mathrm{MRT}} = \frac{\mathbf{h}_3^*}{\|\mathbf{h}_3^*\|}$, and then by plugging it into (5), the receive beamformer $\mathbf{w}_r$ can be obtained by solving

$$\max_{\|\mathbf{w}_r\|=1} |\mathbf{w}_r^\dagger\mathbf{h}_2|^2, \quad \text{s.t} \quad \mathbf{w}_r^\dagger\mathbf{H}_{\mathrm{SI}}\mathbf{h}_3^* = 0. \quad (13)$$

By using similar steps as in the TZF design, the combining vector $\mathbf{w}_r$ is obtained as

$$\mathbf{w}_r^{\mathrm{ZF}} = \frac{\mathbf{D}\mathbf{h}_2}{\|\mathbf{D}\mathbf{h}_2\|}, \quad (14)$$

where $\mathbf{D} = \boldsymbol{I}_{N_R} - \frac{\mathbf{H}_{\mathrm{SI}}\mathbf{h}_3^*\mathbf{h}_3^T\mathbf{H}_{\mathrm{SI}}^\dagger}{\|\mathbf{H}_{\mathrm{SI}}\mathbf{h}_3^*\|^2}$.

C. MRC/MRT Scheme

As an alternative beamforming design, we consider MRC/MRT scheme, where receive and transmit beamforming vectors are matched to the receive and transmit link at the STx. Mathematically speaking, the receive and transmit beamforming vectors with MRC/MRT scheme are set as

$$\mathbf{w}_r^{\mathrm{MRC}} = \frac{\mathbf{h}_2}{\|\mathbf{h}_2\|}, \text{ and } \mathbf{w}_t^{\mathrm{MRT}} = \frac{\mathbf{h}_3^*}{\|\mathbf{h}_3^*\|}, \quad (15)$$

respectively. It is worth mentioning that MRT/MRC scheme is suitable for low complexity FD systems as they do not need to estimate the SI channel. Moreover, MRT/MRC scheme is preferred for HD scenarios and hence it is interesting to characterize its achievable performance in the FD case [24].

IV. PERFORMANCE ANALYSIS

In this section, we characterize the performance of the primary and secondary networks with proposed beamforming designs. Specifically, we derive the delay-constrained throughput of the system and derive outage probability expressions.

A. Delay-Constrained Throughput

We consider the delay-constrained scenario, where the source transmits at a constant rate R_c bits/sec/Hz. The average delay-constrained throughput of the primary and secondary networks with proposed beamforming schemes can be computed as [6]

$$R_{D,\mathrm{PU}}^{\mathrm{i}} = \left(1-\mathrm{P}_{\mathrm{out,PU}}^{\mathrm{i}}\right)R_c(1-\alpha), \quad (16)$$

and

$$R_{D,\mathrm{SU}}^{\mathrm{i}} = \left(1-\mathrm{P}_{\mathrm{out,SU}}^{\mathrm{i}}\right)R_c(1-\alpha), \quad (17)$$

where $\mathrm{P}_{\mathrm{out,PU}}^{\mathrm{i}}$ and $\mathrm{P}_{\mathrm{out,SU}}^{\mathrm{i}}$ are the outage probability of the primary and secondary networks, respectively, and $\mathrm{i} \in \{\mathrm{TZF}, \mathrm{RZF}, \mathrm{MRC}, \mathrm{HD}\}$. Therefore, in order to evaluate the delay-constrained throughput of the considered system, we need to derive the exact outage probability of the system. In the following, we provide outage probability expressions for the primary and

secondary networks, which are used to drive the delay-constrained throughput.

B. Outage Probability Analysis

Outage probability is an important performance metric for wireless networks, which is defined as the probability that the instantaneous SINR falls below a predefined threshold. Let $\theta_1 = 2^{\mathcal{R}_1} - 1$ and $\theta_2 = 2^{\mathcal{R}_2} - 1$, where $\mathcal{R}_1$ and $\mathcal{R}_2$ are the transmission rates at primary and secondary networks, respectively.

An outage event at the primary network occurs when STx fails to decode x_{PR} (A_1^i), or STx can decode x_{PR} but PRx detect x_{SR} incorrectly (A_2^i), or PRx detect x_{SR} but decode x_{PR} incorrectly (A_3^i). Therefore, the outage probability of the PRx can be mathematically expressed as

$$\mathrm{P}_{\mathrm{out,PU}}^{\mathrm{i}} = \mathcal{P}_1^i + \left(1 - \mathcal{P}_1^i\right)\left(1 - \mathcal{P}_2^i\right), \tag{18}$$

where $\mathrm{i} \in \{\mathrm{TZF}, \mathrm{RZF}, \mathrm{MRC}\}$, $\mathcal{P}_1^i = \mathbf{Pr}(\mathrm{A}_1^i)$ and $\mathcal{P}_2^i = \mathbf{Pr}(\overline{\mathrm{A}}_2^i \cap \overline{\mathrm{A}}_3^i)$.

Furthermore, the outage event at the SRx is happened when the SRx's SINR falls below a predetermined threshold, θ_2, which is mathematically expressed as

$$\mathrm{P}_{\mathrm{out,SU}}^{\mathrm{i}} = \mathbf{Pr}\left(\gamma_{\mathrm{SR}}^i < \theta_2\right). \tag{19}$$

In what follows, we present key results for the outage performance of the system with proposed beamforming schemes.

1) TZF Scheme

By Substituting $\mathbf{w}_t^{\mathrm{ZF}}$ into (8) and (9), the SINR $\gamma_{\mathrm{PR},x_{\mathrm{SR}}}^{\mathrm{TZF}}$ and $\gamma_{\mathrm{PR}}^{\mathrm{TZF}}$ are respectively given by

$$\gamma_{\mathrm{PR},x_{\mathrm{SR}}}^{\mathrm{TZF}} = \frac{c_0\|\mathbf{h}_1\|^2\|\tilde{\mathbf{h}}_3\|^2}{c_1\|\mathbf{h}_1\|^2\|\tilde{\mathbf{h}}_3\|^2+\sigma_{\mathrm{PR}}^2}, \tag{20}$$

$$\gamma_{\mathrm{PR}}^{\mathrm{TZF}} = \frac{c_1}{\sigma_{\mathrm{PR}}^2}\|\mathbf{h}_1\|^2\|\tilde{\mathbf{h}}_3\|^2. \tag{21}$$

By substituting $\mathbf{w}_r^{\mathrm{MRC}}$ and $\mathbf{w}_t^{\mathrm{ZF}}$ into (5), the SINR $\gamma_{\mathrm{ST}}^{\mathrm{TZF}} = c_2\|\mathbf{h}_2\|^2$ is obtained. Where $c_0 = \beta_{h_3}\beta_{h_1}a_2\kappa P_{\mathrm{EA}}$, $c_1 = \beta_{h_3}\beta_{h_1}a_1\kappa P_{\mathrm{EA}}$, and $c_2 = \beta_{h_2}\rho_{\mathrm{PT}}$ with $\rho_{\mathrm{PT}} = \frac{P_{\mathrm{PT}}}{\sigma_{\mathrm{ST}}^2}$. The main result for TZF design is provided in the following proposition.

Proposition 1: The exact outage probability of the primary network with the TZF design at the FD STx, is obtained as

$$\mathrm{P}_{\mathrm{out,PU}}^{\mathrm{TZF}} = P\left(N_R, \frac{\theta_2}{c_2}\right) + \mathrm{Q}\left(N_R, \frac{\theta_2}{c_2}\right)\left(1 - \frac{2}{\Gamma(N_R)}\sum_{m=0}^{N_T-2}\frac{\mu^{\frac{N_R+m}{2}}}{m!}K_{N_R-m(2\sqrt{\mu})}\right). \tag{22}$$

where $P(\mathrm{a}, x) = \frac{\gamma(a,x)}{\Gamma(a)}$, $\mathrm{Q}(\mathrm{a}, x) = \frac{\Gamma(a,x)}{\Gamma(a)}$, and $\mu = \max\left(\frac{\sigma_{\mathrm{PR}}^2\theta_1}{c_0 - c_1\theta_1}, \frac{\sigma_{\mathrm{PR}}^2\theta_1}{c_1}\right)$.

Proof: See Appendix A. ■

We now look into the high SNR regime to get more insights on the system design.

Proposition 2: In the high SNR regime, i.e., $\rho_{\mathrm{PT}} \to \infty$, the outage probability of the primary network with the TZF design can be approximated as

$$\mathrm{P}_{\mathrm{out,PU}}^{\infty,\mathrm{TZF}} \approx 1 - \left(\frac{2}{\Gamma(N_R)}\sum_{m=0}^{N_T-2}\frac{\mu^{\frac{N_R+m}{2}}}{m!}K_{N_R-m(2\sqrt{\mu})}\right) \times \left(1 - \Psi_{\mathrm{TZF}}\left(\frac{1}{\rho_{\mathrm{PT}}}\right)^{N_R}\right)$$

$$\underset{\rho_{\mathrm{PT}} \to \infty}{\to} 1 - \left(\frac{2}{\Gamma(N_R)}\sum_{m=0}^{N_T-2}\frac{\mu^{\frac{N_R+m}{2}}}{m!}K_{N_R-m(2\sqrt{\mu})}\right), \tag{23}$$

where $\Psi_{\mathrm{TZF}} = \frac{1}{\Gamma(N_R+1)}\left(\frac{\theta_2}{\beta_{h_2}}\right)^{N_R}$.

Proof: See Appendix B. ■

Proposition 2 indicates that the TZF scheme achieves a floor at high SNR regime and thus exhibits a zero-diversity order behavior.

In order to derive the outage performance of the secondary network, we first need to obtain $\gamma_{\mathrm{SR}}^{\mathrm{TZF}}$. To this end, by substituting $\mathbf{w}_t^{\mathrm{TZF}}$ into (10), $\gamma_{\mathrm{SR}}^{\mathrm{TZF}}$ can be derived as

$$\gamma_{\mathrm{SR}}^{\mathrm{TZF}} = \frac{c_3\|\mathbf{h}_1\|^2\left|\mathbf{h}_4^{\mathrm{T}}\mathbf{w}_t^{\mathrm{ZF}}\right|^2}{c_4\|\mathbf{h}_1\|^2\left|\mathbf{h}_4^{\mathrm{T}}\mathbf{w}_t^{\mathrm{ZF}}\right|^2+\sigma_{\mathrm{SR}}^2}, \tag{24}$$

where $c_3 = \beta_{h_4}\beta_{h_1}a_2\kappa P_{\mathrm{EA}}$, and $c_4 = \beta_{h_4}\beta_{h_1}a_1\kappa P_{\mathrm{EA}}$.

Proposition 3: The exact outage probability of the secondary network with the TZF design can be obtained as

$$\mathrm{P}_{\mathrm{out,SU}}^{\mathrm{TZF}} = 1 - \frac{2\xi^{\frac{N_R}{2}}}{\Gamma(N_R)}K_{N_R}\left(2\sqrt{\xi}\right). \tag{25}$$

where $\xi = \frac{\sigma_{\mathrm{SR}}^2\theta_2}{c_3 - c_4\theta_2}$.

Proof: See Appendix C. ■

2) RZF Scheme

By Substituting $\mathbf{w}_t^{\mathrm{MRT}}$ into (8) and (9), the SINR $\gamma_{\mathrm{PR},x_{\mathrm{SR}}}^{\mathrm{RZF}}$ and $\gamma_{\mathrm{PR}}^{\mathrm{RZF}}$ are respectively given by

$$\gamma_{\mathrm{PR},x_{\mathrm{SR}}}^{\mathrm{RZF}} = \frac{c_0\|\mathbf{h}_1\|^2\|\mathbf{h}_3\|^2}{c_1\|\mathbf{h}_1\|^2\|\mathbf{h}_3\|^2+\sigma_{\mathrm{PR}}^2}, \tag{26}$$

$$\gamma_{\mathrm{PR}}^{\mathrm{RZF}} = \frac{c_1}{\sigma_{\mathrm{PR}}^2}\|\mathbf{h}_1\|^2\|\mathbf{h}_3\|^2. \tag{27}$$

Moreover, by substituting $\mathbf{w}_r^{\mathrm{ZF}}$ and $\mathbf{w}_t^{\mathrm{MRT}}$ into (5), the SINR at the STx is obtained as

$$\gamma_{\mathrm{ST}}^{\mathrm{RZF}} = c_2\|\tilde{\mathbf{h}}_2\|^2. \tag{28}$$

In the following the outage analyses of RZF scheme is provided.

Proposition 4: The exact outage probability of primary network with RZF design is obtained as

$$\mathrm{P}_{\mathrm{out,PU}}^{\mathrm{RZF}} = P\left(N_R - 1, \frac{\theta_2}{c_2}\right) + \mathrm{Q}\left(N_R - 1, \frac{\theta_2}{c_2}\right)\left(1 - \frac{2}{\Gamma(N_R)}\sum_{m=0}^{N_T-1}\frac{\mu^{\frac{N_R+m}{2}}}{m!}K_{N_R-m(2\sqrt{\mu})}\right). \tag{29}$$

Proof: Proof follows similar steps to the proof of

Proposition 1 and thus has been omitted due to space limitation. ■

To get more insight about the effect of system parameters, we develop an asymptotic expression for the outage probability of the primary network with RZF scheme.

Proposition 5: The outage probability of the primary network with RZF scheme in the high SNR regime, i.e., $\rho_{\mathrm{PT}} \to \infty$, can be approximated as

$$\mathrm{P}_{\mathrm{out,PU}}^{\infty,\mathrm{TZF}} \approx 1-\left(\frac{2}{\Gamma(N_R)}\sum_{m=0}^{N_T-1}\frac{\mu^{\frac{N_R+m}{2}}}{m!}K_{N_R-m(2\sqrt{\mu})}\right) \times\left(1-\Psi_{\mathrm{RZF}}\left(\frac{1}{\rho_{\mathrm{PT}}}\right)^{N_R-1}\right) \underset{\rightarrow}{\rho_{\mathrm{PT}}\to\infty} 1-\left(\frac{2}{\Gamma(N_R)}\sum_{m=0}^{N_T-1}\frac{\mu^{\frac{N_R+m}{2}}}{m!}K_{N_R-m(2\sqrt{\mu})}\right), \tag{30}$$

where $\Psi_{\mathrm{RZF}}=\frac{1}{\Gamma(N_R)}\left(\frac{\theta_2}{\beta_{h_2}}\right)^{N_R-1}$.

Proof: The proof follows similar steps as in Proposition 2, thus have been omitted. ■

From (30) we see that the RZF design exhibits a zero-diversity order behavior. Moreover, by comparing (30) and (23), it is clear that RZF scheme outperforms TZF scheme at high SNR regime.

Furthermore, one can readily show that $\gamma_{\mathrm{SR}}^{\mathrm{RZF}}$ have the same statistics as $\gamma_{\mathrm{SR}}^{\mathrm{TZF}}$, and therefore $\mathrm{P}_{\mathrm{out,SU}}^{\mathrm{RZF}}=\mathrm{P}_{\mathrm{out,SU}}^{\mathrm{TZF}}$.

3) MRC/MRT Scheme

With this scheme, $\gamma_{\mathrm{PR},x_{\mathrm{SR}}}^{\mathrm{MRC}}$ and $\gamma_{\mathrm{PR}}^{\mathrm{MRC}}$ are the same as $\gamma_{\mathrm{PR},x_{\mathrm{SR}}}^{\mathrm{RZF}}$ and $\gamma_{\mathrm{PR}}^{\mathrm{RZF}}$, respectively. Furthermore, by substituting $\mathbf{w}_t^{\mathrm{MRT}}$ and $\mathbf{w}_r^{\mathrm{MRC}}$ into (5) we have

$$\gamma_{\mathrm{ST}}^{\mathrm{MRC}}=\frac{c_5\|\mathbf{h}_2\|^2}{c_6\|\mathbf{h}_1\|^2\left|\mathbf{w}_r^{\mathrm{MRC}\dagger}\mathrm{H}_{\mathrm{SI}}\mathbf{w}_t^{\mathrm{MRT}}\right|^2+\sigma_{\mathrm{PR}}^2}. \tag{31}$$

For notational convenience, we define $c_5=\beta_{h_2}P_{\mathrm{PT}}$ and $c_6=\beta_{h_1}\kappa P_{\mathrm{EA}}$.

Proposition 6: The exact outage probability of the primary network with MRC/MRT design is given by

$$\mathrm{P}_{\mathrm{out,PU}}^{\mathrm{MRC}}=I(\theta_2)+\left(1-I(\theta_2)\right)\left(1-\frac{2}{\Gamma(N_R)}\sum_{m=0}^{N_T-1}\frac{\mu^{\frac{N_R+m}{2}}}{m!}K_{N_R-m(2\sqrt{\mu})}\right), \tag{32}$$

where $I(\theta_2)=\frac{2}{\Gamma^2(N_R)}\int_0^{\infty}\left(\frac{c_5x-\theta_2\sigma_{\mathrm{ST}}^2}{\theta_2\sigma_{\mathrm{SI}}^2c_6}\right)^{\frac{N_R}{2}}K_{N_R}\left(2\sqrt{\frac{c_5x-\theta_2\sigma_{\mathrm{ST}}^2}{\theta_2\sigma_{\mathrm{SI}}^2c_6}}\right)x^{N_R-1}\times e^{-x}dx$.

Proof: See Appendix D. ■

Although the integral $I(\theta_2)$ does not seem to admit a closed-form solution, it can be evaluated numerically using software packages like Matlab and Mathematica. We now derive a closed-form lower bound on the outage probability of the primary network with MRC/MRT design.

Corollary 1: The outage probability of the primary user with MRC/MRT design is lower bounded as

$$\mathrm{P}_{\mathrm{out,PU}}^{\mathrm{MRC}}\approx 1-\left(1-\frac{\Gamma(2N_R)}{\Gamma(N_R)}\left(\frac{c_5}{\theta_2\sigma_{\mathrm{SI}}^2c_6}\right)^{\frac{N_R-1}{2}}e^{\frac{c_5}{2c_6\theta_2\sigma_{\mathrm{SI}}^2}}\times W_{\frac{1}{2}-\frac{3}{2}N_R,\frac{N_R}{2}}\left(\frac{c_5}{\theta_2\sigma_{\mathrm{SI}}^2c_6}\right)\right)\left(\frac{2}{\Gamma(N_R)}\sum_{m=0}^{N_T-1}\frac{\mu^{\frac{N_R+m}{2}}}{m!}K_{N_R-m(2\sqrt{\mu})}\right). \tag{33}$$

Proof: See Appendix E. ■

Now, we proceed to calculate $\mathrm{P}_{\mathrm{out,SU}}^{\mathrm{MRC}}$. By inspecting $\gamma_{\mathrm{SR}}^{\mathrm{MRC}}$, it can be seen that $\gamma_{\mathrm{SR}}^{\mathrm{MRC}}$ has the same statistics as $\gamma_{\mathrm{SR}}^{\mathrm{TZF}}$, then it can be readily concluded that $\mathrm{P}_{\mathrm{out,SU}}^{\mathrm{MRC}}=\mathrm{P}_{\mathrm{out,SU}}^{\mathrm{TZF}}$.

V. HALF-DUPLEX TRAMNSMISION

In this section, results for the HD spectrum sharing system is provided. HD system is served as a benchmark to evaluate the performance gains achieved by the FD operation.

In the HD spectrum sharing system, STx is assumed to be HD. We first provide a brief description of the HD spectrum sharing signal model. The energy harvesting phase is the same as the FD spectrum sharing system. For the information transmission phase, the remaining $(1-\alpha)$ portion of block time is equally partitioned into two time slots. Thus, the transmit power at the STx can be expressed as

$$P_{\mathrm{ST}}^{\mathrm{HD}}=\frac{E_{\mathrm{ST}}\alpha T}{\frac{(1-\alpha)T}{2}}=\kappa'\beta_{h_1}P_{\mathrm{EA}}\|\mathbf{h}_1\|^2, \tag{34}$$

where $\kappa'=\frac{2\eta\alpha}{1-\alpha}$.

During the first time slot of the information transmission phase, the received signal at the STx is given by

$$y_{\mathrm{ST},2}[i]=\sqrt{\beta_{h_2}P_{\mathrm{PT}}}\mathbf{w}_r^{\dagger}\mathbf{h}_2x_{\mathrm{PR}}[i]+\mathbf{w}_r^{\dagger}\mathbf{H}_{\mathrm{SI}}\mathbf{w}_tx_R[i]+n_{\mathrm{ST}}[i]. \tag{35}$$

Therefore, the required SNR at ST to decode the x_{PR} is given by

$$\gamma_{\mathrm{ST}}^{\mathrm{HD}}=\frac{\beta_{h_2}P_{\mathrm{ST}}\left|\mathbf{w}_r^{\dagger}\mathbf{h}_2\right|^2}{\sigma_{\mathrm{ST}}^2}. \tag{36}$$

During the second time slot, STx transmits a superimposed signal to the PRx and SRx. The received signals at PRx and SRx are given by

$$y_{\mathrm{PR}}[i]=\sqrt{\beta_{h_3}P_{\mathrm{ST}}^{\mathrm{HD}}}\mathbf{h}_3^T\mathbf{w}_tx_R[i]+n_{\mathrm{PR}}[i], \tag{37}$$

and

$$y_{\mathrm{SR}}[i]=\sqrt{\beta_{h_4}P_{\mathrm{ST}}^{\mathrm{HD}}}\mathbf{h}_4^T\mathbf{w}_tx_R[i]+n_{\mathrm{SR}}[i], \tag{38}$$

respectively. Therefore, the SINR at the PRx for decoding x_{SR} is given by

$$\gamma_{\mathrm{PR},x_{\mathrm{SR}}}^{\mathrm{HD}}=\frac{\beta_{h_3}\beta_{h_1}a_2\kappa'P_{\mathrm{EA}}\|\mathbf{h}_1\|^2|\mathbf{h}_3^T\mathbf{w}_t|^2}{\beta_{h_3}\beta_{h_1}a_1\kappa'P_{\mathrm{EA}}\|\mathbf{h}_1\|^2|\mathbf{h}_3^T\mathbf{w}_t|^2+\sigma_{\mathrm{PR}}^2}. \tag{39}$$

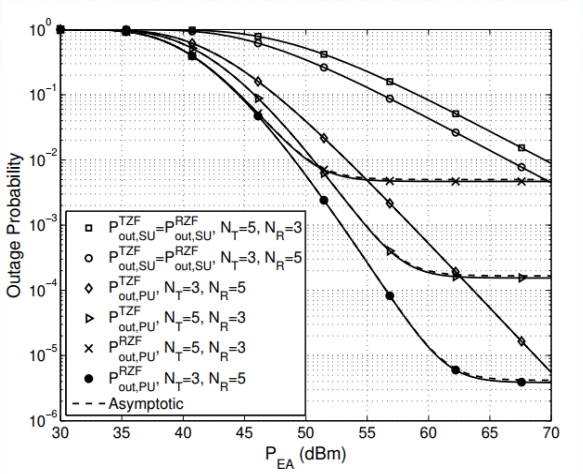

Fig. 2. Outage probability of the primary and secondary networks with TZF and RZF beamforming schemes and for different antenna configurations (P_{PT} =10 dBm).

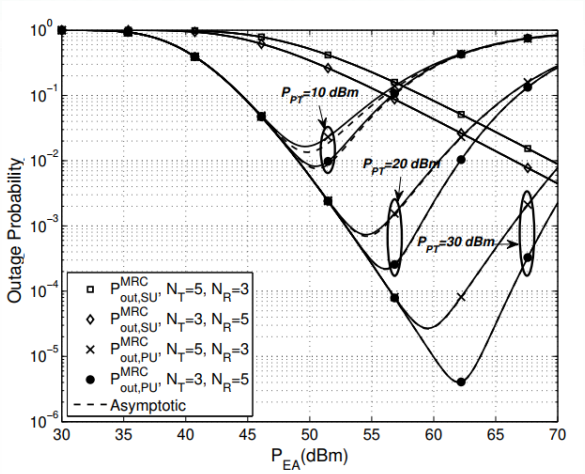

Fig. 3. Outage probability of the primary and secondary networks versus P_{EA} for MRC scheme and for different antenna configurations.

Moreover, the required SNR at PRx for decoding its information is given by

$$\gamma_{PR}^{HD} = \frac{\beta_{h_3}\beta_{h_1}a_1\kappa' P_{EA}}{\sigma_{PR}^2}\|\mathbf{h}_1\|^2|\mathbf{h}_3^T\mathbf{w}_t|^2. \quad (40)$$

Furthermore, the required SINR at the SRx for extracting its own massage is as following

$$\gamma_{SR}^{HD} = \frac{\beta_{h_4}\beta_{h_1}a_2\kappa' P_{EA}\|\mathbf{h}_1\|^2|\mathbf{h}_4^T\mathbf{w}_t|^2}{\beta_{h_4}\beta_{h_1}a_1\kappa' P_{EA}\|\mathbf{h}_1\|^2|\mathbf{h}_4^T\mathbf{w}_t|^2+\sigma_{SR}^2}. \quad (41)$$

We now analyze the outage probability of primary and secondary networks under HD transmission. We note that in case of HD transmission, the MRC/MRT beamforming design is the optimum scheme. Therefore, the receive and transmit beamformers are designed as

$$\mathbf{w}_r^{MRC} = \frac{\mathbf{h}_2}{\|\mathbf{h}_2\|},$$
$$\mathbf{w}_t^{MRT} = \frac{\mathbf{h}_3^*}{\|\mathbf{h}_3^*\|}. \quad (42)$$

In the following, we present the results for the HD transmission mode.

Proposition 7: The outage probability of primary user in HD mode is given by

$$P_{out,PU}^{HD,MRC} = P\left(N_R, \frac{\theta_1}{c_2}\right) + Q\left(N_R, \frac{\theta_1}{c_2}\right) \times \left(1 - \frac{2}{\Gamma(N_R)}\sum_{m=0}^{N_T-1}\frac{\mu'^{\frac{N_R+m}{2}}}{m!}K_{N_R-m}\left(2\sqrt{\mu'}\right)\right). \quad (43)$$

where $\mu' = \max\left(\frac{\sigma_{PR}^2\theta_1}{2c_0-2c_1\theta_1}, \frac{\sigma_{PR}^2\theta_1}{2c_1}\right)$.

Proof: The proof of this proposition follows the same approach as proof of Proposition 1, thus it's been omitted. ■

Proposition 8: The outage probability of secondary user in HD mode and with MRC scheme is given by

$$P_{out,SU}^{HD,MRC} = 1 - \frac{2\xi'^{\frac{N_R}{2}}}{\Gamma(N_R)}K_{N_R}\left(2\sqrt{\xi'}\right), \quad (44)$$

where $\xi' = \frac{\sigma_{SR}^2\theta_2}{2c_3-2c_4\theta_2}$.

Proof: The proof of this proposition is as same as the proof of Proposition 3, thus it have been dropped. ■

VI. NUMERICAL RESULTS AND DISCUSSION

In this section, numerical and simulation results are provided to confirm the correctness of the outage probability analysis. The network setting is as follows. The distance between PTx-STx, EAP-STx, STx-PRx, and STx-SRx are set to 100m, 10m, 20m, and 100m, respectively. According to [25], commercial chips are now available for tens of microwatts (μW) RF power transferred over 12 m. Thus, we consider that EAP is placed close to the STx. The path loss exponent of the links, the TS parameter, and RF-to-DC conversion efficiency are set to m =3, α =0.5, and η =0.7, respectively. Furthermore, all the noise variances are set to -80 dBm. The power allocation factors of NOMA users are set to a_1 =0.1 and a_2 =0.9[1].

Fig. 2 investigates the outage probability of primary and secondary networks in terms of P_{EA} for TZF and RTF schemes when P_{PT}=10 dBm. These curves are depicted for different set of antennas. As shown, when the N_R increases, the outage probability of the secondary network decreases and acts independently from N_T. The asymptotic results based on (23) and (30) are also presented. In the case that N_R decreases from 5 to 3, and N_T increases from 3 to 5, it can be seen that the outage probability of the TZF scheme gets better at the low values of P_{EA}, and at the high values of P_{EA}, the outage of the TZF and RZF schemes have growth. This is because the amount of

[1] Optimizing NOMA power allocation coefficients dynamically according to the users' channel conditions can further enhance the performance gain of NOMA assisted system. This subject goes beyond the scope of the current paper but constitutes an interesting future work.

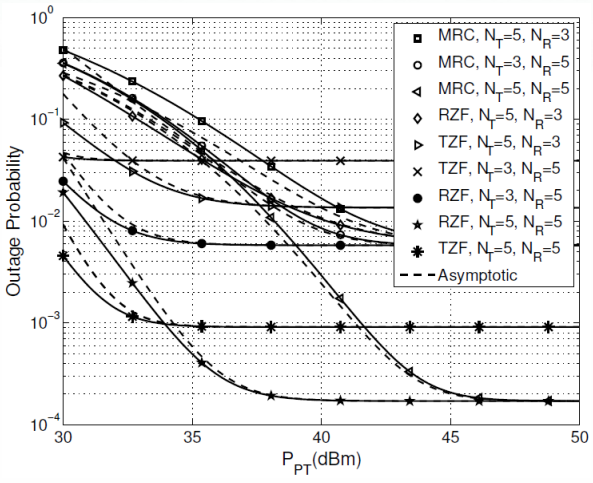

Fig. 4. Primary network's outage probability versus $\boldsymbol{P_{PT}}$ for TZF, RZF, and MRC schemes with $\boldsymbol{P_{EA}} = 30$ dBm.

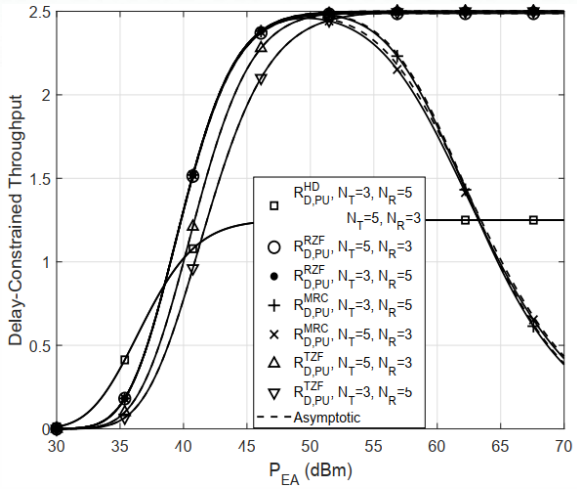

Fig. 5. Delay-constrained throughput of the primary network versus $\boldsymbol{P_{EA}}$ for different beamforming design ($\boldsymbol{R_c}$= 5 bits/s/Hz, and $\boldsymbol{P_{PT}} = 10$ dBm).

harvested power at the STx gets decreased as N_R decreases. As a result, the received SINRs at the PRx reduce.

Fig. 3 illustrates the outage probability of the MRC scheme versus P_{EA}. The outage probability is drawn for different values of P_{PT}, and different antennas configurations. As shown, the outage probability of the MRC scheme for secondary network decreases when N_R increases. Also, there is an optimum P_{EA} in which minimum value of the outage probability is achieved. For the P_{EA} beneath the optimum value, the outage probabilities of primary network decrease with the same slop. If the P_{EA} exceeds its optimum value the outage probabilities start to increase. The optimum value of P_{EA} increases as P_{PT} increases. Additionally, when N_R increases, the optimum value of P_{EA} get increased.

Fig. 4 shows the outage probability of the primary network versus P_{PT} for the proposed TZF, RZF, and MRC schemes. This figure is depicted for different antennas configuration, when P_{EA}= 30 dBm. As this figure represents, the more N_R and N_T get, the lower the outage probability we have. Furthermore, among these schemes, RZF outperforms the two other schemes when N_R increases. Also, the asymptotic expressions are depicted, which shows they are well-set with analytical expressions in the high values of P_{PT}.

Fig. 5 shows the achieved delay-constrained throughput of the primary network versus the power of energy access point and for two antenna configurations. Moreover, the delay-constrained throughput of the HD counterpart is also included. It is obvious that RZT scheme is superior in terms of delay-constrained throughput in low values of P_{EA}. Moreover, the delay-constrained throughput of the primary network with RZF and TZF tends to a constant value at high P_{EA}values due to the outage probability floor exhibited in Fig. 2. In the MRC scheme it is evident that in power values lower than optimum value, the delay-constrained throughput of MRC scheme follows the same trend as RZF scheme but at power values greater than that optimum value, the delay-constrained throughput of MRC scheme is decreased due to the degradation of its outage probability (as shown in Fig. 3).

Fig. 6 shows the delay-constrained throughput of the secondary network versus P_{EA} and for FD and HD systems. It is clear that by increasing the number of receive antennas from 3 to 5, the delay-constrained throughput of the secondary network is improved. This is due to the fact that by increasing the number of receive antennas the ability of energy harvesting at the STx is improved.

Fig. 7 demonstrates the delay-constrained throughput of the system versus α for different antenna configurations. Due to the complexity of the involved outage probability expressions, a closed-form solution of the optimal α that maximizes (16) and (17) is not possible. Instead, the optimal value of α can be numerically evaluated through the Monte Carlo simulations. In Fig. 7, case_1 denotes to $N_T = 5$ and $N_R = 5$, case_2 denotes to $N_T = 3$ and $N_R = 5$ and case_3 denotes to $N_T = 5$ and $N_R = 3$. It is clear that increasing in N_T and N_R significantly improve the performance. Moreover, when α is increased the delay-constrained throughput of system is increased until α achieves its optimum value, then the delay-constrained throughput of the system decreases. This is due to the fact that increasing α more that its optimum value causes decrement of transmission time of the information. Furthermore, it could be realized that optimum value of α is decreased as N_T and N_R increased.

VII. CONCLUSION

In this paper, we have investigated delay-constrained throughput of a wireless-powered FD spectrum-sharing network with NOMA transmissions. We proposed two ZF-based linear beamforming designs at the FD STx to mitigate the SI. We derived the exact and asymptotic expressions for the outage probability of the primary and secondary networks. The results indicated that the ZF-beamforming schemes reach considerable outage performance compared to the

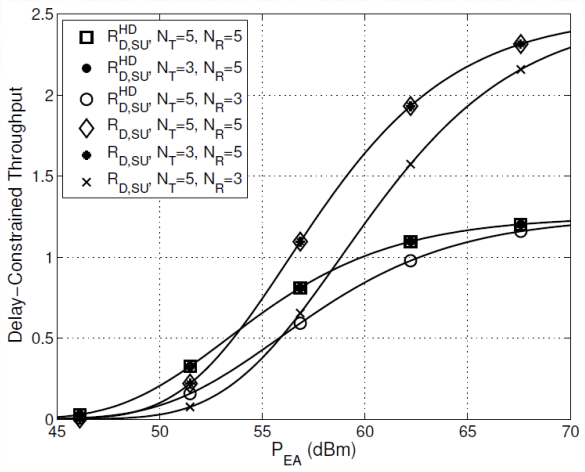

Fig. 6. Delay-constrained throughput of the secondary network versus $\boldsymbol{P_{EA}}$ for different beamforming design ($\boldsymbol{R_c}$ = 5 bits/s/Hz, and $\boldsymbol{P_{PT}}$ = 10 dBm).

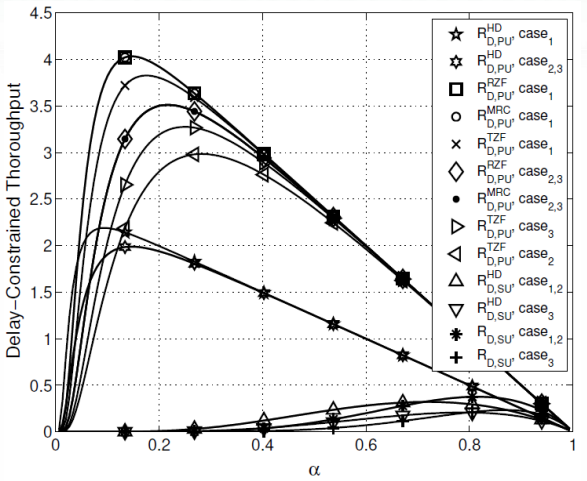

Fig. 7. Delay-constrained throughput of the primary and secondary network versus α and for different beamforming design (R_c =5 bits/s/Hz, P_{PT} = 10 dBm, and P_{EA} = 30 dBm).

benchmark beamforming design, MRC/MRT. Moreover, we perceived that the performance gap between the system can be further increased by deploying more receive antennas at the STx.

APPENDIX A

PROOF OF PROPOSITION 1

We start with the characterization of $\mathcal{P}_2^{\mathrm{TZF}}$, which can be expressed as

$$\begin{aligned}\mathcal{P}_2^{\mathrm{TZF}} &= \mathbf{Pr}\left(\frac{c_0\|\mathbf{h}_1\|^2\|\tilde{\mathbf{h}}_3\|^2}{c_1\|\mathbf{h}_1\|^2\|\tilde{\mathbf{h}}_3\|^2+\sigma_{\mathrm{PR}}^2}>\theta_1,\right.\\ &\qquad \left.\frac{c_1\|\mathbf{h}_1\|^2\|\tilde{\mathbf{h}}_3\|^2}{\sigma_{\mathrm{PR}}^2}>\theta_2\right),\\ &= \mathbf{Pr}\left(\|\mathbf{h}_1\|^2\|\tilde{\mathbf{h}}_3\|^2>\mu\right). \end{aligned} \quad (45)$$

Noticing that $\|\mathbf{h}_1\|^2 \sim \chi_{2N_R}$, its pdf is given by $f_{\|\mathbf{h}_1\|^2}(x)=\frac{1}{\Gamma(N_R)}x^{N_R-1}e^{-x}$. On the other hand, according to [6], the $\|\tilde{\mathbf{h}}_3\|^2$ is also a Chi-squared RV with $2(N_T-1)$ d.o.f with cdf given by $F_{\|\tilde{\mathbf{h}}_3\|^2}(x)=\frac{1}{\Gamma(N_T-1)}\gamma(N_T-1,x)$. Hence, by using $f_{\|\mathbf{h}_1\|^2}(x)$ and $F_{\|\tilde{\mathbf{h}}_3\|^2}(x)$, the probability $\mathcal{P}_2^{\mathrm{TZF}}$ in (45) can be expressed as

$$\mathcal{P}_2^{\mathrm{TZF}} = 1-\frac{1}{\Gamma(N_R)\Gamma(N_T-1)}\int_0^{\infty}\gamma(N_T-1,\tfrac{\mu}{x})x^{N_R-1}e^{-x} \quad (46)$$

By applying the series expansion of the incomplete Gamma function in [23, Eq.(8.352.1)], (46) can be written as

$$\mathcal{P}_2^{\mathrm{TZ}} = 1-\frac{1}{\Gamma(N_R)}\int_0^{\infty}\left(1-e^{-\frac{\mu}{x}}\sum_{m=0}^{N_T-2}\frac{\mu^m}{x^m m!}\right)\times x^{N_R-1}e^{-x}dx. \quad (47)$$

Then, after some simple algebraic manipulation and applying [23, Eq.(3.471.9)] we get

$$\mathcal{P}_2^{\mathrm{TZF}} = \frac{2}{\Gamma(N_R)}\sum_{m=0}^{N_T-2}\frac{\mu^{\frac{N_R+m}{2}}}{m!}K_{N_R-m}(2\sqrt{\mu}). \quad (48)$$

Now, we turn our attention to $\mathcal{P}_1^{\mathrm{TZF}}$. According to $\gamma_{\mathrm{ST}}^{\mathrm{TZF}}=c_2\|\mathbf{h}_2\|^2$ where $\|\mathbf{h}_2\|^2\sim\chi_{2N_R}$, Therefore, $\mathcal{P}_1^{\mathrm{TZF}}$ can be readily obtained as

$$\mathcal{P}_1^{\mathrm{TZF}} = \frac{1}{\Gamma(N_R)}\gamma\left(N_R,\frac{\theta_2}{c_2}\right). \quad (49)$$

By plugging (48) and (49) into (18), we arrive at the desired result in (22).

APPENDIX B

PROOF OF PROPOSITION 2

By inspecting (23), it is evident that when N_R is increased the outage probability of the PRx is decreased. By invoking the series representation of Gamma function in [23, Eq.(8.354.1)] and substituting into $P\left(N_R,\frac{\theta_2}{c_2}\right)$, and by omitting the high-order exponent, The asymptotic $P\left(N_R,\frac{\theta_2}{c_2}\right)$ can be obtained as $P\left(N_R,\frac{\theta_2}{c_2}\right)\approx\Psi_{\mathrm{TZF}}\left(\frac{1}{\rho_{\mathrm{PT}}}\right)^{N_R}$.

At the end, substituting $\Psi_{\mathrm{TZF}}\left(\frac{1}{\rho_{\mathrm{PT}}}\right)^{N_R}$ into (18), we achieve the desired result in (23).

APPENDIX C

PROOF OF PROPOSITION 3

According to (19) we have

$$\begin{aligned}\mathrm{P}_{\mathrm{out,SU}}^{\mathrm{TZF}} &= \mathbf{Pr}\left(\frac{c_3\|\mathbf{h}_1\|^2\left|\mathbf{h}_4^T\mathbf{w}_t^{\mathrm{ZF}}\right|^2}{c_4\|\mathbf{h}_1\|^2\left|\mathbf{h}_4^T\mathbf{w}_t^{\mathrm{ZF}}\right|^2+\sigma_{\mathrm{SR}}^2}<\theta_2\right),\\ &= \mathbf{Pr}\left(\|\mathbf{h}_1\|^2\left|\mathbf{h}_4^T\mathbf{w}_t^{\mathrm{ZF}}\right|^2<\xi\right) \end{aligned} \quad (50)$$

Given that $\left|\mathbf{h}_4^T\mathbf{w}_t^{\mathrm{ZF}}\right|^2$ follows exponential distribution[26], for $\theta_2 < \frac{c_3}{c_4}$ we have

$$\mathrm{P}_{\mathrm{out,SU}}^{\mathrm{TZF}} = \int_0^{\infty} \frac{1}{\Gamma(N_R)} \gamma\left(N_R, \frac{\xi}{x}\right) e^{-x} dx. \quad (51)$$

Now, by utilizing [23, Eq. (6.453)], we obtain the desired result in (25).

APPENDIX D

PROOF OF PROPOSITION 6

By using the same steps to proof of Proposition 1, $\mathcal{P}_2^{\mathrm{MRC}}$ can be expressed as

$$\mathcal{P}_2^{\mathrm{MRC}} = \frac{2}{\Gamma(N_R)} \sum_{m=0}^{N_T-1} \frac{\mu^{\frac{N_R+m}{2}}}{m!} K_{N_R-m}(2\sqrt{\mu}). \quad (52)$$

According to (31),$\|\mathbf{h}_2\|^2 \sim \chi_{2N_R}$, $\|\mathbf{h}_1\|^2 \sim \chi_{2N_R}$ and $\left|\mathbf{w}_r^{\mathrm{MRC}\dagger}\mathbf{H}_{\mathrm{SI}}\mathbf{w}_t^{\mathrm{MRT}}\right|^2$ follows exponential distribution [27]. Therefore, $\mathcal{P}_1^{\mathrm{MRC}}$ can be written as

$$\mathcal{P}_1^{\mathrm{MRC}} = \mathbf{Pr}\left(\frac{c_5\|\mathbf{h}_2\|^2}{c_6\|\mathbf{h}_1\|^2\left|\mathbf{w}_r^{\mathrm{MRC}\dagger}\mathbf{H}_{\mathrm{SI}}\mathbf{w}_t^{\mathrm{MRT}}\right|^2 + \sigma_{\mathrm{ST}}^2} < \theta_2\right),$$
$$= \frac{1}{\Gamma^2(N_R)} \int_0^{\infty}\int_0^{\infty} x^{N_R-1} y^{N_R-1} e^{-\frac{c_5 x - \theta_2\sigma_{\mathrm{ST}}^2}{\theta_2\sigma_{\mathrm{SI}}^2 c_6 y}} e^{-x} \times e^{-y} dx dy. \quad (53)$$

By applying [23, Eq. (3.471.9)] we have

$$\mathcal{P}_1^{\mathrm{MRC}} = \frac{1}{\Gamma^2(N_R)} \int_0^{\infty} 2\left(\frac{c_5 x - \theta_2\sigma_{\mathrm{ST}}^2}{\theta_2\sigma_{\mathrm{SI}}^2\theta_6}\right)^{\frac{N_R}{2}} \times K_{N_R}\left(2\sqrt{\frac{c_5 x - \theta_2\sigma_{\mathrm{ST}}^2}{\theta_2\sigma_{\mathrm{SI}}^2 c_6}}\right) x^{N_R-1} e^{-x} dx. \quad (54)$$

Finally, by substituting (52) and (54) into (18), we achieve the desired result in (32).

APPENDIX E

PROOF OF COROLLARY 1

By ignoring the noise term of the $\gamma_{\mathrm{ST}}^{\mathrm{MRC}}$, $\tilde{\mathcal{P}}_1^{\mathrm{MRC}}$ can be upper bounded as

$$\tilde{\mathcal{P}}_1^{\mathrm{MRC}} < \frac{1}{\Gamma^2(N_R)} \int_0^{\infty} 2\left(\frac{c_5 x}{\theta_2\sigma_{\mathrm{SI}}^2 c_6}\right)^{\frac{N_R}{2}} \times K_{N_R}\left(2\sqrt{\frac{c_5 x}{\theta_2\sigma_{\mathrm{SI}}^2 c_6}}\right) x^{N_R-1} e^{-x} dx. \quad (55)$$

Now by applying the integral identity [23, Eq. (6.643.3)], the integral (55) can be solved as

$$\tilde{\mathcal{P}}_1^{\mathrm{MRC}} < \frac{\Gamma(2N_R)}{\Gamma(N_R)} \left(\frac{c_5}{\theta_2\sigma_{\mathrm{SI}}^2 c_6}\right)^{\frac{N_R-1}{2}} e^{\frac{c_5}{2\theta_2\sigma_{\mathrm{SI}}^2 c_6}} \times W_{\frac{1}{2}-\frac{3}{2}N_R, \frac{N_R}{2}}\left(\frac{c_5}{\theta_2\sigma_{\mathrm{SI}}^2 c_6}\right). \quad (56)$$

Finally, substituting (52) and (56) into (18) yields the desired result.

REFERENCES

[1] A. Sabharwal, P. Schniter, D. Guo, D. W. Bliss, S. Rangarajan, and R. Wichman, "In-band full-duplex wireless: Challenges and opportunities," *IEEE J. Sel. Areas Commun.*, vol. 32, pp. 1637–1652, Sep. 2014.J. Clerk Maxwell, A Treatise on Electricity and Magnetism, 3rd ed., vol. 2. Oxford: Clarendon, 1892, pp.68–73.

[2] M. Duarte, "Full-duplex wireless: Design, implementation and characterization," Ph.D. dissertation, Dept. Elect. and Computer Eng., Rice University, Houston, TX, 2012.

[3] L. Laughlin, M. A. Beach, K. A. Morris, and J. L. Haine, "Optimum single antenna full duplex using hybrid junctions," *IEEE J. Sel. Areas Commun.*, vol. 32, pp. 1653–1661, Sep. 2014.

[4] T. Riihonen, S. Werner, and R. Wichman, "Mitigation of loopback self-interference in full-duplex MIMO relays," *IEEE Trans. Signal Process.*, vol. 59, pp. 5983–5993, Dec. 2011.

[5] H. A. Suraweera, I. Krikidis, G. Zheng, C. Yuen, and P. J. Smith, "Low-complexity end-to-end performance optimization in MIMO full-duplex relay systems," *IEEE Trans. Wireless Commun.*, vol. 13, no. 2, pp. 913–927, Jan. 2014.

[6] M. Mohammadi, B. K. Chalise, H. A. Suraweera, C. Zhong, G. Zheng, and I. Krikidis, "Throughput analysis and optimization of wireless-powered multiple antenna full-duplex relay systems," *IEEE Trans. Commun.*, vol. 64, no. 4, pp. 1769–1785, Apr. 2016.

[7] S. Haykin, "Cognitive radio: Brain-empowered wireless communications," *IEEE J. Sel. Areas Commun.*, vol. 23, no. 2, pp. 201–220, Feb. 2005.

[8] R. Manna, R. H. Y. Louie, Y. Li, and B. Vucetic, "Cooperative spectrum sharing in cognitive radio networks with multiple antennas," *IEEE Trans. Signal Process.*, vol. 59, pp. 5509–5522, Nov 2011.

[9] H. Kim, S. Lim, H. Wang, and D. Hong, "Optimal power allocation and outage analysis for cognitive full duplex relay systems," *IEEE Trans. Wireless Commun.*, vol. 11, pp. 3754–3765, Oct. 2012.

[10] M. Amjad, F. Akhtar, M. H. Rehmani, M. Reisslein, and T. Umer, "Full-duplex communication in cognitive radio networks: A survey," *IEEE Commun. Surveys Tutorials*, vol. PP, no. 99, pp. 1–1, 2017.

[11] Y. Saito, Y. Kishiyama, A. Benjebbour, T. Nakamura, A. Li, and K. Higuchi, "Non-orthogonal multiple access (NOMA) for cellular future radio access," in *Proc. IEEE 77th Veh. Technol. Conf. (VTC'13)*, Dresden, Germany, June 2013, pp. 1–5.

[12] Z. Ding, X. Lei, G. K. Karagiannidis, R. Schober, J. Yuan, andV. K. Bhargava, "A survey on non-orthogonal multiple accessfor 5G networks: Research challenges and future trends," *IEEE J. Sel. Areas Commun.*, vol. 35, no. 10, pp. 2181–2195, Oct. 2017.

[13] M. Mohammadi,X. Shi, B. K. Chalise, Z. Ding, H. A. Suraweera, C. Zhong, and J. S. Thompson, ``Full-duplex non-orthogonal multiple access for next generation wireless systems", *IEEE Communications Magazine*, vol. 57, pp. 110-116, May 2019.

[14] Z. Mobini, M. Mohammadi, H. A. Suraweera, and Z. Ding, "Full-duplex multi-antenna relay assisted cooperative nonorthogonal multiple access," in *Proc. IEEE Global Commun. Conf. (GLOBECOM 17) ´* , Singapore, Dec 2017, pp. 1–7.

[15] L. Lv, J. Chen, and Q. Ni, "Cooperative non-orthogonal multiple access in cognitive radio," *IEEE Commun. Lett.*, vol. 20, pp. 2059–2062, Oct. 2016.

[16] Y. Liu, Z. Ding, M. Elkashlan, and J. Yuan, "Nonorthogonal multiple access in large-scale underlay cognitive radio networks," *IEEE Trans. Veh. Technol.*, vol. 65, pp. 10 152–10 157, Dec. 2016.

[17] L. Lv, J. Chen, Q. Ni, and Z. Ding, "Design of cooperative non-orthogonal multicast cognitive multiple access for 5G systems: User scheduling and performance analysis," *IEEE Trans. Commun.*, vol. 65, pp. 2641–2656, June 2017.

[18] M. Mohammadi, B. K. Chalise, A. Hakimi, H. A. Suraweera, and Z. Ding, "Joint beamforming design and power allocation for full-duplex NOMA cognitive relay systems," in Proc.

IEEE Global Commun. Conf. (GLOBECOM'17) , Singapore, Dec 2017, pp. 1-7.

[19] S. Buzzi, C. I, T. E. Klein, H. V. Poor, C. Yang, and A. Zappone, "A survey of energy-efficient techniques for 5G networks and challenges ahead," *IEEE J. Sel. Areas Commun.*, vol. 34, pp. 697–709, Apr. 2016.

[20] S. Bi, Y. Zeng, and R. Zhang, "Wireless powered communication networks: An overview," *IEEE Wireless Commun. Mag.*, vol. 23, no. 2, pp. 10–18, Apr. 2016.

[21] Y. Alsaba, C. Y. Leow, and S. K. A. Rahim, "Full-duplex cooperative non-orthogonal multiple access with beamforming and energy harvesting," *IEEE Access*, vol. 6, pp. 19 726–19 738, 2018.

[22] P. Deng, B. Wang, W. Wu, and T. Guo, "Transmitter design in MISO-NOMA system with wireless-power supply," *IEEE Commun. Lett.*, vol. 22, pp. 844–847, Apr. 2018.

[23] I. S. Gradshteyn and I. M. Ryzhik, *Table of Integrals, Series and Products*, 7th ed. Academic Press, 2007.

[24] M. Mohammadi, B. K. Chalise, A. Hakimi, Z. Mobini, H. A. Suraweera, and Z. Ding, "Beamforming design and power allocation for full-duplex non-orthogonal multiple access cognitive relaying," *IEEE Trans. Commun.*, vol. 66, pp. 5952–5965, Dec. 2018.

[25] Wireless Power Solutions-Powercast Corp. [Online]. Available: http://www.powercastco.com.

[26] M. Mohammadi, H. A. Suraweera, and C. Tellambura, "Uplink/downlink rate analysis and impact of power allocation for full-duplex cloud-RANs," *IEEE Trans. Wireless Commun.*,vol. 17, pp. 5774 – 5788, Sept. 2018.

[27] A. Hakimi, M. Mohammadi, and Z. Mobini, "Outage probability of wireless powered multiantenna cooperative spectrum sharing networks with full-duplex and NOMA transmissions," *in 9th International Symposium on Telecommunications (IST)*, *IEEE*, pp. 127-132, Dec. 2018.

Azar Hakimi received the B.Sc. and the M.Sc. degrees in Electrical Engineering from the Shahrekord University, Iran, in 2015 and 2018, respectively. Her research interests are in the areas of Cognitive Radio Cooperative Communication Systems, Wireless Information and Power Transfer, and Non-Orthogonal Multiple Access Communications.

Mohammadali Mohammadi (S'09, M'15) received the B.S. degree in Electrical Engineering from the Isfahan University of Technology, Isfahan, Iran, in 2005, and the M.Sc. and Ph.D. degrees in the same Electrical Engineering from K. N. Toosi University of Technology, Tehran, Iran in 2007 and 2012, respectively. From November 2010 to November 2011, he was a visiting researcher in the Research School of Engineering, the Australian National University, Australia, working on Cooperative Networks. He is currently an Associate Professor in the Faculty of Engineering, Shahrekord University, Iran. His main research interests include Cooperative Communications, Energy Harvesting and Green Communications, Full-Duplex Communications and Stochastic Geometry.

Zahra Mobini (S'09, M'15) received the B.Sc. degree in Electrical Engineering from Isfahan University of Technology, Isfahan, Iran, in 2006, and the M.Sc. and Ph.D. degrees, both in Electrical Engineering, from the M. A. University of Technology and K. N. Toosi University of Technology, Tehran, Iran, respectively. From November 2010 to November 2011, she was a Visiting Researcher at the Research School of Engineering, Australian National University, Canberra, ACT, Australia. She is currently an Assistant Professor with the Faculty of Engineering, Shahrekord University, Shahrekord, Iran. Her research interests include Wireless Communication Systems, Cooperative Networks, and Network Coding.